PERGAMON

International Journal of Solids and Structures 40 (2003) 555–571

INTERNATIONAL JOURNAL OF SOLIDS and STRUCTURES

www.elsevier.com/locate/ijsolstr

Element-failure concepts for dynamic fracture and delamination in low-velocity impact of composites

T.E. Tay *, V.B.C. Tan, M. Deng

Department of Mechanical Engineering and Division of Bioengineering, National University of Singapore, 10 Kent Ridge Crescent, Singapore 119260, Singapore

Received 18 May 2002; received in revised form 10 October 2002

Abstract

An element-failure algorithm is proposed and incorporated into a finite element code for simulating dynamic crack propagation and impact damage in laminated composite materials. In this algorithm, when a crack is propagating within a finite element, the element is deemed to have partially failed, but not removed from the computations. Consequently, only a fraction of the stresses that were computed before the crack tip entered the element contribute to the nodal forces of the element. When the crack has propagated through the element, the element is completely failed and therefore can only resist volumetric compression. This treatment of crack propagation in isotropic solids allows fracture paths within individual elements and is able to accommodate crack growth in any arbitrary direction without the need for remeshing. However, this concept is especially powerful when extended to the modeling of damage and delamination in fibre-reinforced composite laminates. This is because the nature of damage in composite laminates is generally diffused, characterized by multiple matrix cracks, fibre pullout, fibre breakage and delaminations. It is usually not possible to define or identify crack tips in the tradition of fracture mechanics. Since parts of a damaged composite structure are often able to partially transmit load despite the presence of some damage, it is advantageous to model the damaged portions with partially failed elements. The damage may be efficiently modeled and tracked using element-failure concepts, with the application of appropriate failure criteria and damage evolution laws. The idea is to embody the effects of damage into the effective nodal forces of the finite element. In this paper, we report the novel use of element-failure concepts in the analysis of low-velocity impact damage of composite laminates. The initiation and propagation of delaminations arising from the impact are predicted and the results show qualitative agreement with experimental observation of the formation of multiple delaminations in impact-damaged specimens. While such delaminations do not permit transmission of tensile stress waves across the cracked surfaces, transmission of compressive stress waves are allowed in the simulation. It is further shown that, when elements are allowed to fail, the dynamic stress wave distributions are altered significantly. In the element-failure algorithm, the issue of interpenetration of delamination surfaces in the model does not arise. This is a significant advantage over the conventional method of explicitly modeling the delamination surfaces and crack front, where generally, much computational time must be spent in employing contact algorithms to ensure physically admissible solutions. Finally, we also demonstrate the simulation of crack propagation of pre-notched specimens of an isotropic material under initial conditions of mode II loading using

* Corresponding author. Fax: +65-6779-1459.
E-mail address: mpetayte@nus.edu.sg (T.E. Tay).

0020-7683/02/$ - see front matter
PII: S0020-7683(02)00623-6

the element-failure algorithm. The numerical results showed that the cracks propagated at an angle of about 70° with respect to the notches, in agreement with the experimental results of Kalthoff.

Keywords: Element-failure; Delamination; Damage; Composites; Finite element; Low-velocity impact

1. Introduction

Computational simulation of dynamic crack propagation using the finite element method is often restricted to cases where the crack path is known a priori. In the traditional Lagrangian finite element method, once the material is discretized into a fixed set of elements, it is difficult to create new surfaces within the materials unless the new surface coincides with element boundaries. Hence, crack growth in arbitrary directions would require some form of remeshing to realign elements around the crack tip to the direction of crack growth. While remeshing can be carried out easily if the crack path does not change abruptly (Lim et al., 1996; Samoa, 1981; Murti, 1986), the remapping of variables from original to new mesh is computationally intensive and always results in the loss of accuracy due to dispersion and distortion.

In situations where the crack path is known a priori, it is possible to generate a finite element mesh where the crack path is along element edges to eliminate the need for remeshing. Two classes of finite element crack propagation technique based on this scheme are the nodal release technique (Rousselier, 1979) and the nodal splitting technique (Bakuckas et al., 1995). The nodal release technique is useful in cases where the crack propagates along a plane or line of symmetry. In such cases, the plane of symmetry is modeled as a symmetric displacement boundary condition in the FE mesh. A node anchored to the boundary initially represents the crack tip. As the crack propagates the node is "released" from the boundary. When the crack path does not lie on any symmetric plane the nodal splitting technique is commonly employed. A finite element mesh is generated with the crack path sandwiched between two rows of elements. Crack growth is effected by allowing elements on opposite sides of the crack to separate. Nodes common to elements on either side of crack are "split" in the process. Instantaneous release and splitting of nodes are equivalent to sudden release of finite amounts of energy. This results in severe nodal oscillations. To minimize such noise, nodes that are released or split do not become traction free immediately. Instead, internal nodal forces acting on the nodes prior to nodal release or nodal splitting are gradually reduced to zero (Bakuckas et al., 1995; Dexter and O'Donoghue, 1993).

Beissel et al. (1998) extended the concept of nodal release and nodal splitting along element edges to crack propagation within elements of an FE mesh and proposed an element-failure algorithm. In this algorithm, cracks are allowed to propagate through an element. When a crack is propagating within an element, the element is deemed to have partially failed. Such elements are not removed from the finite element computations. However, only a fraction of the stresses that were computed before the crack tip entered the element contribute to the nodal forces of the element. This fraction is dependent on the crack length within the element. When the crack has propagated through the element, the element is completely failed and can only resist volumetric compression. This treatment of crack propagation allows fracture paths within individual elements and hence can accommodate crack growth in arbitrary direction without the need for remeshing. However, the analysis presented in the paper by Beissel et al. (1998) was essentially that of mode I fracture. In this paper, we report on the simulation of crack propagation of pre-notched specimens under initial conditions of mode II loading using the element-failure algorithm, and investigate the dependency of results on fineness of the mesh. Kalthoff (1988) and Kalthoff and Winkler (1988) performed an extensive range of such experiments and his results will serve to verify the element-failure algorithm.

The main aim of this paper, however, is to show that the element-failure concept and algorithm is particularly suited for dynamic failure analysis of composite structures, where certain modes of failure do not completely preclude the ability of the composite material to sustain stresses. It is well known that damage in composite materials is generally complicated and consists of multiple failure modes, such as fibre breakage, fibre pullout, delamination between plies, matrix cracking, fibre–matrix debonding, etc. More than one of these failure modes are often present in damaged composite structures. They have strong interactions with one another so that usually it is not possible to clearly identify and define a single crack in the traditional fracture mechanics sense. Even in exceptional situations where a crack may be defined, such as in the case of a single delamination, other mechanisms such as fibre bridging across the crack surfaces and crack kinking or branching usually greatly complicate the analysis. In cases involving dynamic loading such as in ballistic impact, the additional consideration of strain-rate dependency of the material properties may have to be taken into account. However, despite the increased level of complexity of the analysis, most of these mechanisms have the advantageous effect of improving the apparent fracture toughness and damage tolerance of composite structures. Unless there is complete separation of the material, the damaged part of the structure can often partially sustain stresses. The role of damage mechanics is to provide information for the evolution of damage modes and their effect on the constitutive relations of the material. This information can be programmed into the element-failure algorithm in modeling the damage progression in dynamically loaded composite structures. Through the relatively simple example of initiation and propagation of delamination damage in low-velocity impact of a composite laminate, the advantages of employing element-failure concepts in computational analysis of composites can be illustrated. The methodology used for modeling the Kalthoff specimen is easily extended to the analysis of low-velocity impact of composites. However, it should be pointed out that a consistent general methodology for incorporating damage and fracture mechanics into a three-dimensional element-failure algorithm is not yet available.

2. Element-failure concepts and algorithm

In this section, the concepts and implementation of the element-failure method are described. Most of these are common to both the problem of the Kalthoff specimen and analysis of delamination damage in low-velocity impact of composite laminates. However, in the former, the crack path trajectory is predicted with the aid of the T^* integral and either the maximum hoop stress or maximum principal stress criteria, while in the latter, the Tsai-Wu tensor failure criterion is used for predicting both initiation and propagation of the delaminations.

2.1. Concepts

The concept of using failed elements to model crack propagation was first conceived by Mahishi and Adams (1982). The scheme assumes that when an element of an FE mesh is loaded beyond its maximum strain energy capacity, it fails and is subsequently removed from the mesh and omitted from further computation. The stiffness associated with the element is also reduced to zero. Loads that were sustained by the element prior to failure are then transferred to surrounding elements.

The element-failure algorithm formulated by Beissel et al. (1998) is different from the concept proposed by Mahishi and Adams (1982) in that elements are not physically removed from the FE mesh. Beissel's definition of a failed element is one with a crack traversing completely across it. New surfaces are created but material is not removed. The difference between a failed element and a deleted element is that a failed element can still sustain compressive loads while a deleted element is a complete void in the material.

An element in the element fail algorithm is in one of three states—undamaged, partially failed and completely failed. A completely failed element is one with a crack extending from one edge of the element to another edge. A partially failed element is one that contains a fracture but is not severed into two, i.e. the crack tip resides in a partially failed element. Undamaged elements are those that do not contain any cracks. All elements are able to resist compression. Partially failed elements are only partly able to resist volumetric expansion. Once a crack propagates into an element, the tensile and shear load bearing capability of the element is reduced. This reduction is linearly proportional to the crack length within the element. When the crack has propagated through the entire element, the element is deemed to have completely failed and can only resist compression.

The element-failure concept has not been widely applied to composite materials and structures, to the best of the authors' knowledge. However, here the concept is particularly useful, as partially failed elements can effectively model the damage in composite structures. The authors are currently investigating a mechanistic-based failure theory for use with element-failure algorithms, with the aim of analyzing the evolution of damage in the form of matrix cracks and delaminations. Damage in the form of matrix cracking has previously been modeled with a constitutive damage law and applied to the problem of a composite plate with a centrally located hole, loaded under quasi-static monotonically increasing tension (Tay et al., 1997). The concepts outlined in Tay et al. (1997) may be extended to three-dimensional finite element stress analysis of damaged composite structures.

2.2. Implementation

Once appropriate criteria governing crack growth, crack tip trajectory and crack tip velocity are available, the incorporation of the element-failure algorithm into finite element codes is simple. Essentially, in finite element algorithms for dynamic problems, the following quantities are updated in sequence until the computation is terminated—nodal displacement; element strains; element stresses; nodal forces; nodal accelerations; nodal velocities; and back to nodal displacements again. The element-failure algorithm only affects the portion of the FE code that determines the nodal forces from the element stresses. Undamaged elements are not affected by the algorithm and their nodal forces are determined in the usual manner,

$$\mathbf{f} = \int_{\Omega_e} \mathbf{B}^{\mathrm{T}} \boldsymbol{\sigma} \, \mathrm{d}\Omega. \tag{1}$$

Here, the integration is performed over the volume of the element; $\mathbf{B}$ is the usual matrix of the derivatives of the element interpolants and $\boldsymbol{\sigma}$ is the Cauchy stress tensor.

For completely failed elements, the nodal forces are non-zero only when the elements are under compression. In such situations, the pressure within the element is computed from constitutive relations between pressure and volumetric strain. Hydrostatic compression occurs when the elements undergo negative volumetric strain. The total strain of within each failed element of the mesh is decomposed into the deviatoric and volumetric components. By only retaining negative volumetric strains in the determination of element stresses, the nodal forces of a failed element due purely to hydrostatic compression can be determined without any other special algorithm. The FE routine for determining the forces through Eq. (1) can be used without modification by considering only the pressure term of the Cauchy stress tensor.

In the case of partially failed elements, only a fraction of the forces computed from Eq. (1) contribute to the element nodal forces, i.e.

$$\mathbf{f} = \alpha \int_{\Omega_e} \mathbf{B}^{\mathbf{T}} \boldsymbol{\sigma} \, \mathrm{d}\Omega, \quad (0 < \alpha < 1). \tag{2}$$

The value of α decreases with depth of crack propagation into the element. It has a value of unity just prior to the crack entering the element and approaches zero when the crack tip exits the element. The gradual decrease in nodal forces as the crack propagates through an element helps to reduce nodal oscillations, a result of sudden release of energy from element deletion. The use of a scalar multiplier such as α in the current form implies isotropic material softening and is probably not appropriate for application to composite laminates in general. Work is currently in progress to determine a more rational methodology to directionally modify nodal forces, accounting for the anisotropic state of damage within the element. The development of a consistent methodology is pursued in parallel with a new micromechanics-based failure theory recently proposed by Gosse (2002).

3. Governing criteria for fracture trajectory

The implementation of appropriate criteria to determine crack initiation, direction of crack growth and velocity of crack propagation is critical to successful dynamic crack propagation simulation. The framework for theoretical elastodynamic fracture has been reported by Rose (1976), Kanninen and Poplar (1985) and Freund (1990) together with some practical applications. Central to the determination of fracture trajectory is the computation of the dynamic stress intensity factor.

In this paper, the T^* integral introduced by Atluri (1982) and Atluri et al. (1984) will be used to characterize the crack tip fields. This integral essentially reflects the flow of energy into the crack tip region and is a measure of energy release associated with a unit area of crack surface extension in dynamic fracture. Its expression in incremental form is given by

$$\Delta T^* = \lim_{\Gamma^* \to 0} \int_{\Gamma^*} [(\Delta W + \Delta T) n_{\mathrm{p}} - (\sigma_{ij} + \Delta\sigma_{ij}) n_j \Delta u_{i,\mathrm{p}} - \Delta\sigma_{ij} n_j u_{i,\mathrm{p}}] \, \mathrm{d}\Gamma, \tag{3}$$

where Γ^* is a contour around the crack tip; ΔW and ΔT are the incremental internal energy density and kinetic energy respectively; n_j is the jth component of the unit normal to the contour Γ^*; n_{p} is the component of the unit normal in the direction of crack propagation; and u_i and σ_{ij} are the usual notations for components of the displacement and stress tensor.

The T^* energy integral is only locally path independent in the sense that path independence is achieved only when the radius Γ^* approaches zero. However, as errors in finite element analyses of fracture are greatest near the crack tip because of the steep gradients in stresses, Eq. (3) is not used in the computation of the T^* integral. The divergence theorem is invoked to equate Eq. (3) to a domain plus contour integral in the computation to give

$$\begin{aligned} \Delta T^* = {} & \int_{\Gamma} [(\Delta W + \Delta T) n_{\mathrm{p}} - (\sigma_{ij} + \Delta\sigma_{ij}) n_j \Delta u_{i,\mathrm{p}} - \Delta\sigma_{ij} n_j u_{i,\mathrm{p}}] \, \mathrm{d}\Gamma + \int_{\Omega} \left[\Delta\sigma_{ij} \left(\varepsilon_{ij,\mathrm{p}} + \frac{1}{2} \Delta\varepsilon_{ij,\mathrm{p}} \right) \right. \\ & \left. - \Delta\varepsilon_{ij} \left(\sigma_{ij,\mathrm{p}} + \frac{1}{2} \Delta\sigma_{ij,\mathrm{p}} \right) \right] \mathrm{d}\Omega + \int_{\Omega} \rho [(\ddot{u}_i + \Delta\ddot{u}_i) \Delta u_{i,\mathrm{p}} - (\dot{u}_i + \Delta\dot{u}_i) \Delta\dot{u}_{i,\mathrm{p}} + \Delta\ddot{u}_i u_{i,\mathrm{p}} - \Delta\dot{u}_i \dot{u}_{i,\mathrm{p}}] \, \mathrm{d}\Omega. \end{aligned} \tag{4}$$

Here, Γ is a contour round the crack tip that is sufficiently far from the tip to avoid steep gradients in stresses and Ω is the domain between Γ^* and Γ as shown in Fig. 1.

Several criteria have been proposed for the prediction of the direction of crack propagation, namely,

(i) minimum strain energy density by Sih (1974),
(ii) maximum energy release rate by Hussain et al. (1974),
(iii) maximum tensile circumferential stress by Erdogan and Sih (1963), and
(iv) ratio of stress intensity factors of mode I and II by Taha and Swartz (1989).

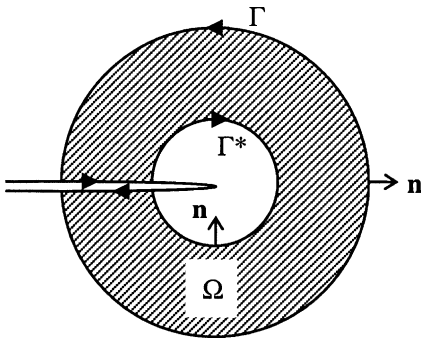

Fig. 1. Domain and boundaries of the T^* energy integral.

Since the value of the T^* integral is dependent upon the direction of crack propagation, the direction which gives the maximum value of T^* can also be used to indicate the direction of crack growth.

For the numerical analyses reported in this paper, the velocity of crack propagation is determined from empirical data which relates the T^* integral to the crack tip velocity (Rosakis and Freund, 1982; Dally et al., 1985), while two criteria for crack propagation direction are investigated—maximum principal stress and maximum hoop stress around the crack tip.

4. Dynamic fracture under in-plane shear loading

Kalthoff and Winkler (1988) performed a series of dynamic fracture tests to understand crack propagation under pure mode II loading. These tests serve as good benchmarks for the simulation of dynamic fracture because it was observed that crack propagation might occur in directions different from the pre-cracks of the test specimens. Two types of steels were investigated—high strength maraging steel and chromium–molybdenum steel. The schematic of their experimental set up is shown in Fig. 2. The specimen to be tested contains two parallel edge pre-cracks of equal length and crack tip radius. A cylindrical projectile with diameter equivalent to the distance between the cracks hits the edge squarely between the pre-cracks. This generates a compressive pulse that propagates to the crack tips causing an initial mode II loading.

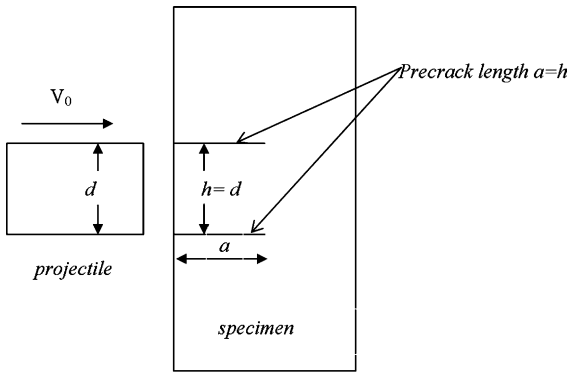

Fig. 2. Schematic of set up for mode II loading in dynamic fracture tests.

The important parameters of the tests are the impact velocity, V_0, and the crack tip radius. High impact velocities and low tip radii increases the strain rate experienced by the material around the crack tip. Unlike cracks subjected to pure mode I loading where the cracks propagate in the direction of perpendicular to the load, the tests performed by Kalthoff and Wrinkler showed that different failure mechanisms occur under different loading conditions. Low impact velocities coupled with large tip radii does not result in any crack propagation because the strain rate is not high enough, hence, pre-cracks remain stable. When either the impact velocity or tip acuity exceeds a certain threshold, the crack will start to propagate. The crack trajectory deviates from the initial direction and propagates at an angle of about 70° outwards to the direction of the original notches. At even higher impact velocities and crack tip acuities, a different failure mechanism occurs; a large amount of the impact energy is expended in the formation localized shear bands. These bands are almost in the same direction of the pre-cracks and are of limited length.

A finite element simulation of mode II loading of pre-notch specimen similar to the tests carried out by Kalthoff was performed using the element-failure algorithm to gauge the capability of the method in predicting crack propagation. The pre-notched specimen is a steel 4340 plate of dimensions 200 × 100 mm. The notch lengths are 50 mm and the crack tip radii are 0.85 mm. The cylindrical impactor has a diameter of 50 mm. It hits the steel specimen with an impact velocity of 39.3 m/s. The plate is discretized into plane stress linear triangle elements with single Gauss points. We have found that square or rectangular elements are not suitable because they tend to over-constrain the crack path such that the prediction is forced to conform to the grid pattern of the mesh. The steel is modeled as an elastic material with Young's modulus of 210 GPa and density of 7860 kg/m^3. Only half the plate is modeled because of symmetry. The mesh around the crack tip is shown in Fig. 3. The entire mesh contains 7081 nodes and 13,924 elements.

In the simulation, the direction of crack propagation is determined by either the maximum principal stress or the maximum hoop stress around the crack tip. Crack growth and crack tip velocity are determined from experimental data reported by Rosakis and Freund (1982) and Dally et al. (1985), which gives a relationship between crack speed and the stress intensity factor as shown in Fig. 4. To utilize this data, the relationship between the stress intensity factor and the T^* integral computed during the computational analysis is used, i.e.

$$K = \sqrt{\frac{ET^*}{1-\nu^2}}. \tag{5}$$

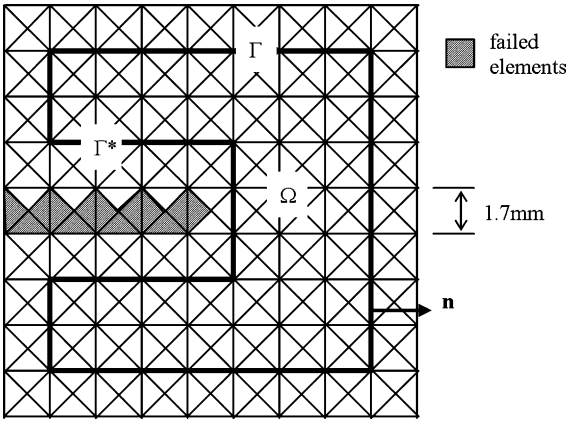

Fig. 3. Linear triangle elements of FE mesh around crack tip.

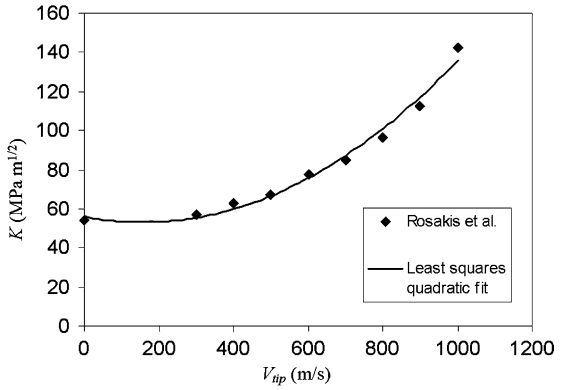

Fig. 4. Stress intensity factor K, against crack tip velocity V_{tip}.

It can be seen from Fig. 4 that the crack tip speed increases exponentially with K, and that the dynamic fracture toughness of the material is about 57 MPa $\text{m}^{1/2}$, i.e. crack growth is arrested at stress intensity factors less than 57 MPa $\text{m}^{1/2}$. The experimental data is fitted with a polynomial given by

$$V_{\text{tip}} = 0.0001K^2 - 0.0375K + 56.0, \tag{6}$$

where the units of V_{tip} and K are (m/s) and (MPa $\text{m}^{1/2}$), respectively.

Although the maximum principal or maximum hoop stress criteria together with the data in Fig. 4 can be used to determine the direction and incremental crack extension at each computational time step and thus predict the entire crack trajectory, this is not implemented because it is computationally expensive. The merits of knowing the exact crack path is also not apparent in the element fail algorithm because all failed elements are treated in the same fashion regardless of the crack orientation within them. Instead of tracing the actual fracture path, two simplifications are adopted. Firstly, the crack propagates in a straight path within elements and hence the trajectory only changes whenever the crack tip leaves an element and enters another. The next simplification is that the distance the crack needs to travel within an element before it exits it is not calculated, instead, an "average" distance is applied to all elements. For our simulation, where triangular elements are used, this distance is reported to be

$$D = \sqrt{2A_{\text{ele}}}, \tag{7}$$

where A_{ele} is the area of the element.

As the crack is propagating within an element, the T^* integral is calculated at each time step and the relation between crack tip velocity and stress intensity factor is used to update the crack length, d, within the element using a central difference integration scheme

$$d^{(n+1)} = d^{(n)} + \Delta t \times V_{\text{tip}}. \tag{8}$$

A linear relationship is assumed to exist between the crack length within a partially failed element, d, and the element's ability to sustain tensile and shear loads. Thus, α in equation is determined from

$$\alpha^{(n)} = \frac{d^{(n)}}{D}. \tag{9}$$

The crack is deemed to have completely propagated through the element when

$$\delta^{(n+1)} = d^{(n+1)} - D \geqslant 0. \tag{10}$$

An adjustment is then made to the time step to correct for the overshoot of the crack tip. Instead of the usual time step Δt, a reduced time step $\Delta t_{\text{reduced}}$ is used to update all variables in the current time step,

$$\Delta t_{\text{reduced}} = \frac{\delta^{(n+1)}}{V_{\text{tip}}}. \tag{11}$$

Eq. (4) is used in the evaluation of the T^* integral. The expression requires the domain integral of derivatives of strains and stresses which are singular at element boundaries in displacement-based finite element methods. The common remedy of averaging the stresses and strains at the nodes is adopted. The stresses and strains are then interpolated from the nodal values in the same manner as displacements.

The direction of crack propagation is determined based on either the maximum principal stress or hoop stress around the crack tip. Since the actual crack path is not tracked in the simulation, it is not necessary to search for the maximum stress at all points around the crack tip; only the stresses at the Gauss points of elements immediately around the element containing the crack tip are checked, i.e. the crack will propagate towards the element with the largest principal or hoop stress. It should be noted that the crack tip is only permitted to propagate into an element which shares a common edge as the existing crack tip element.

The results of the element-failure algorithm simulation are shown in Figs. 5–8. Figs. 5 and 7 are the predictions when the maximum principal stress around the crack tip is used to guide the direction of crack propagation, while Figs. 6 and 8 are the results when the crack is made to propagate in the direction of the maximum hoop stress.

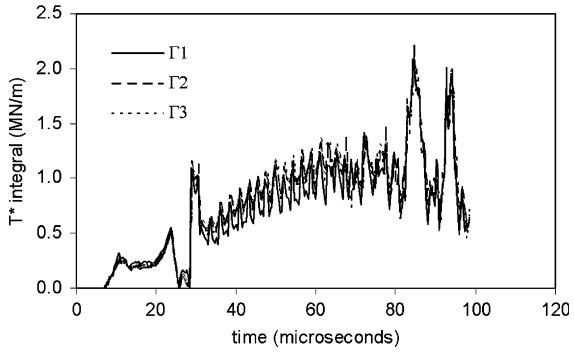

Fig. 5. History of predicted T^* integral using maximum principal stress to determine direction of crack propagation.

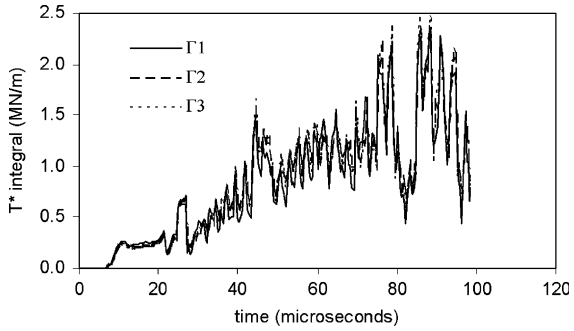

Fig. 6. History of predicted T^* integral using maximum hoop stress to determine direction of crack propagation.

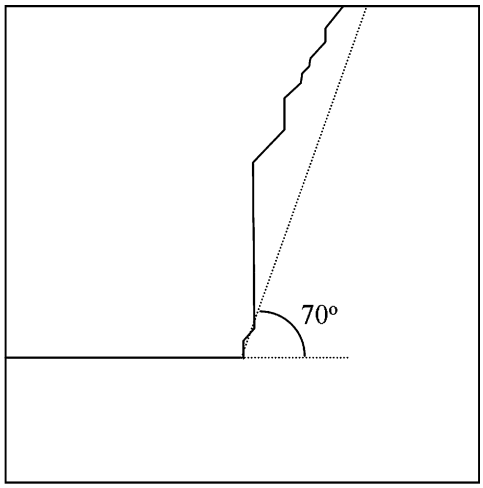

Fig. 7. Predicted fracture trajectory using maximum principal stress to determine direction of crack propagation.

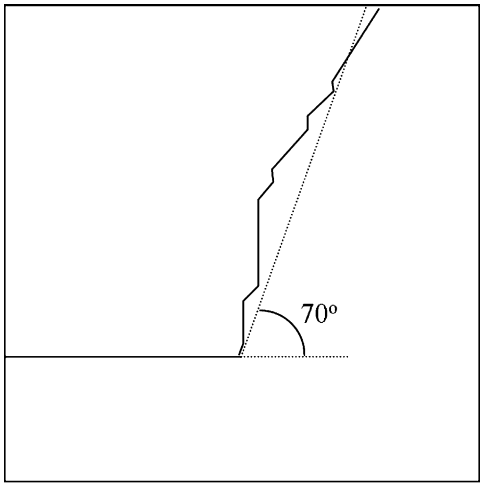

Fig. 8. Predicted fracture trajectory using maximum hoop stress to determine direction of crack propagation.

Figs. 5 and 6 show the T^* integral values driving the crack propagation computed from the simulation. In the simulation, the outer boundary of the T^* integral, Γ, is 6 element lengths, i.e. 6×1.7 mm, from the crack tip. This outer radius is deemed sufficiently far from the crack tip so that it does not suffer from the numerical errors expected near the tip. The inner radius of the T^* domain, Γ^*, is often a concern as the integral is only path independent for a sufficiently small radius. However, too small a radius does not give converging results due to the inherently large errors in stresses near the crack tip. Three inner radii are reported in both Figs. 5 and 6—Γ_1 (1 element length), Γ_2 (2 element lengths) and Γ_3 (3 element lengths). The close agreement of the T^* integral values for the three different inner radii verifies that the computed integral is convergent and path independent.

The oscillations of the T^* integral observed in the simulations occur whenever the crack tip leaves an element and enters another. Beissel et al. (1998) also reported such oscillations in their simulation and

suggested the fluctuations can be reduced by increasing the average fracture length within triangular elements to a maximum of

$$D = 2\sqrt{2A_{\text{ele}}}. \tag{12}$$

Figs. 7 and 8 show the predicted fracture paths when the different criteria are used in determining crack growth direction. The bold lines are the predicted crack trajectories while the dotted lines are the fracture lines observed by Kalthoff and Winkler (1988) in actual tests on different steel specimens under similar conditions. Since the fine details of the crack path are not tracked during the simulation and fracture is approximated by a trail of failed elements, the crack trajectories in the computational simulation resemble more closely a winding path through the centers of failed elements rather than a smooth fracture line. Errors arising from the discretization will definitely have some effects in dynamic fracture problems which are sensitive to small perturbations in crack trajectories. Nevertheless, the predicted fracture paths are close to experimental observations, especially when the maximum hoop stress criterion is used in determining crack growth direction.

Currently, the element-failure algorithm does not trace fracture trajectories but only approximates them. The incorporation of a tracking algorithm can be included in future work so that the actual fracture length of each element can be used in the computation instead of an average value. More directions can also be checked for the determination of crack growth direction other than limiting the search to the directions of neighboring elements around the crack tip.

5. Stress waves and delamination in impact of composites

The preceding element-failure code was applied to study stress wave propagation and delamination initiation and growth in a laminated composite plate under low-velocity impact. The problem consists of a unidirectional laminated composite plate of thickness 5 mm and height 100 mm, fully clamped at the top and bottom edges, impacted in the thickness direction at the center of the plate by a rigid circular cylindrical projectile of radius 2.5 mm, with an incident velocity of 6.5 m/s (Fig. 9). The elastic and strength properties of the unidirectional composite are obtained from Choi et al. (1991), and are reproduced in Table 1. The transverse wave speed w may be estimated by the formula

$$w = \sqrt{\frac{E_{22}}{\rho}} \tag{13}$$

and has a value of 2.43×10^3 m/s. Hence the incident stress wave arising out of initial impact will take about 2.06 μs to travel from the impacted face to the back face.

The two-dimensional finite element model of the plate consists of 32,000 triangular elements, with 20 elements in the thickness direction. The impact due to the projectile is represented and approximated by a short constant pulse of 6.5 m/s applied over a period of 2.5 μs. The results of the finite element analysis without damage are compared to and verified with the results of a separate but identical analysis using the commercial software ABAQUS with the same mesh. For example, in Fig. 10, the stress wave distributions at 2.0 μs after impact using the element-failure code and ABAQUS are shown to be identical.

The Tsai-Wu tensor failure criterion (Tsai, 1992) is used to determine delamination initiation and propagation in the composite laminate. The choice of a general criterion like the Tsai-Wu theory, rather than a more specific but restrictive interlaminar normal stress failure criterion, is intended to illustrate the generality of the approach for modeling damage in composites. Figs. 11–14 show the stress wave distributions and the development of delamination in the laminate for times 3.55, 4.23, 4.36 and 5.01 μs respectively after initial application of the impact pulse. All the stress wave contours shown are for the

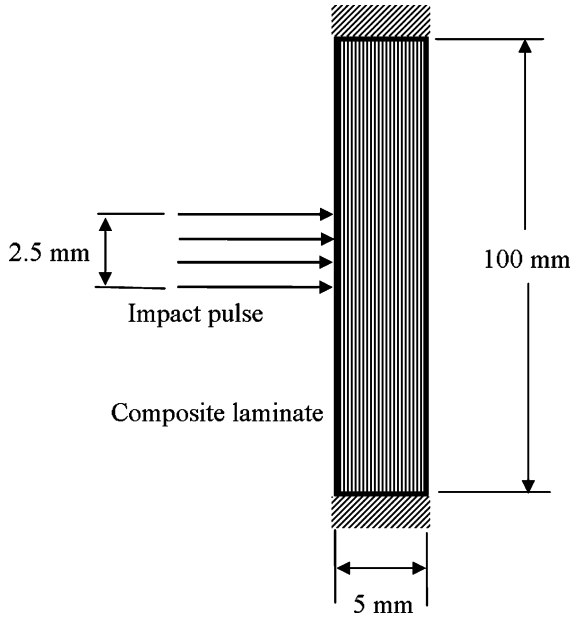

Fig. 9. Low-velocity impact of a composite laminate.

Table 1
Material properties used in the FE simulation, reproduced from Choi et al. (1991)

Property		
Longitudinal (fibre direction) modulus	E_{11}	156 GPa
Transverse modulus	E_{22}	9.09 GPa
Out-of-plane shear modulus	G_{12}	3.24 GPa
Out-of-plane Poisson's ratio	υ_{12}	0.228
Density	ρ	1540 kg/m^3
Longitudinal strength (tension)	X_T	1520 MPa
Longitudinal strength (compression)	X_C	1590 MPa
Transverse strength (tension)	Y_T	45 MPa
Transverse strength (compression)	Y_C	252 MPa
Shear strength	S	105 MPa

normal stress component in the laminate thickness (i.e. impact) direction, and the values are in Pa. The dark shaded areas in Figs. 11(a), 12(a), 13(a), 14(a) represent failed elements.

Fig. 11(a) shows the initiation of delamination in the laminate at 3.55 μs after initial impact. It shows that the first delaminations appear when the stress wave front is returning from the back face, but has not yet reached the front (impacted) face. The stress wave interactions produce localized tensile stress concentrations with magnitudes large enough to initiate delamination, according to the Tsai-Wu criterion. At this stage, the stress contours for the analysis without element-failure (Fig. 11(b)) and the analysis including element-failure (Fig. 11(c)) are almost identical, as expected, since the size of the delaminations is quite small. At 4.23 μs after impact, the stress wave front has just undergone two reflections, one from the back face, and the other from the front face. The stress interactions produce further tensile stress fields in the immediate wake of the stress wave, causing the two existing delaminations to grow, and two other delaminations near the center of the laminate to initiate (Fig. 12(a)). Comparison between Fig. 12(b) and (c)

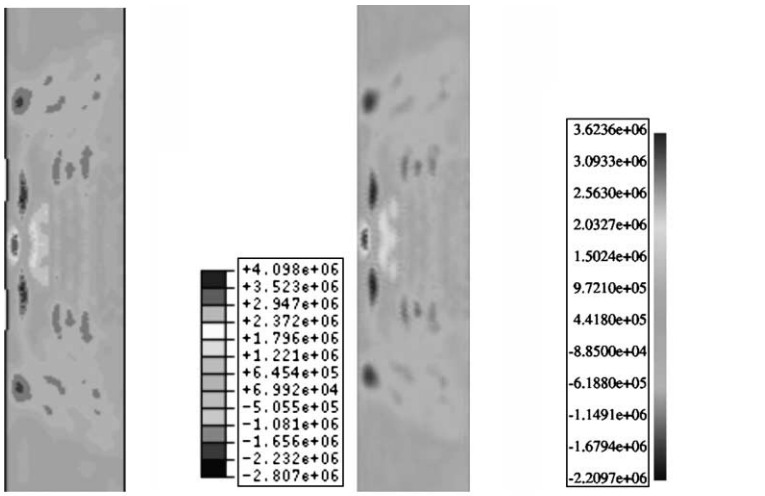

Fig. 10. Verification of element-failure code with ABAQUS, for stress contours 2.0 μs after initial impact and without damage.

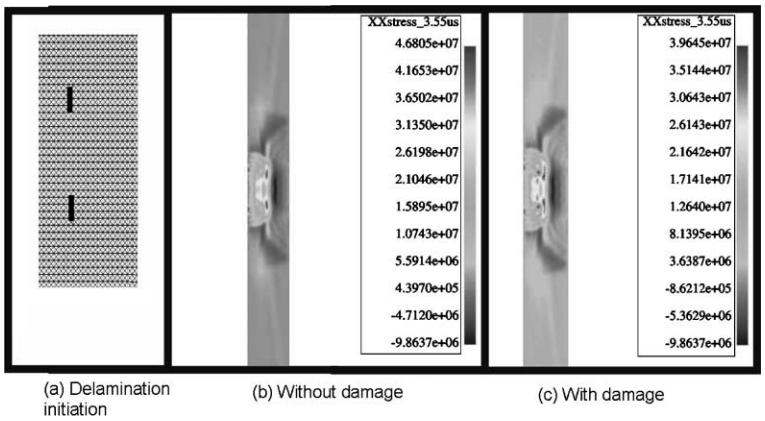

Fig. 11. Damage initiation and stress wave distribution at 3.55 μs after initial impact.

suggests that there are now significant differences in the distribution of stresses. The presence of the failed elements (representing delaminations) causes considerable interference of the interacting stress waves. The failed elements permit transmission of compressive stress waves across the delaminated surfaces, but tensile stress waves incident to the surface of the failed elements are subsequently reflected as compressive waves. In this sense, the elements modeling the delaminated surfaces can be considered as having partially failed, since a delamination crack with compressive normal stresses across its faces would be closed (sometimes referred to as a ''kissing'' delamination), but an open delamination crack would not sustain tensile stresses at its surfaces. In this work, all the elements failed in the tensile mode, although the Tsai-Wu failure criterion allows for the possibility of shear failure. The question of whether a delamination allows for shear transfer is more complicated to answer. In this work, for the sake of simplicity, we have chosen to disallow shear stress transfer after an element has failed. This is a reasonable assumption if the delamination crack is

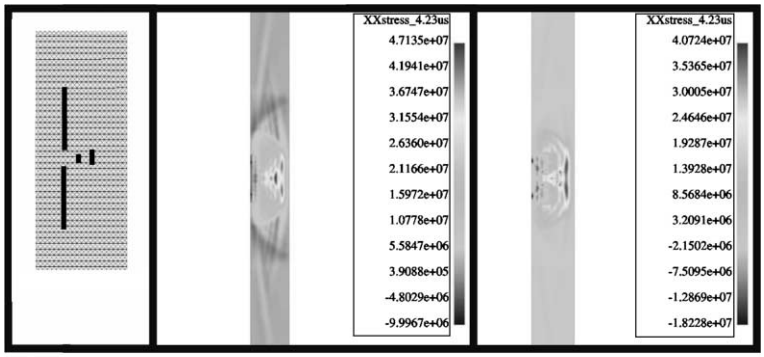

Fig. 12. Damage initiation and stress wave distribution at 4.23 μs after initial impact.

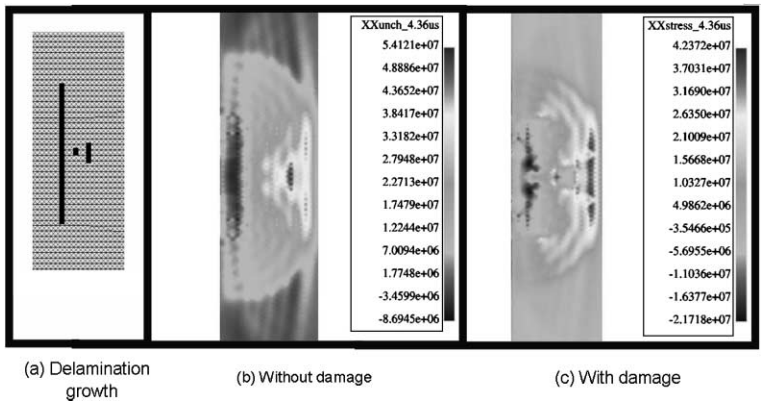

Fig. 13. Damage initiation and stress wave distribution at 4.36 μs after initial impact.

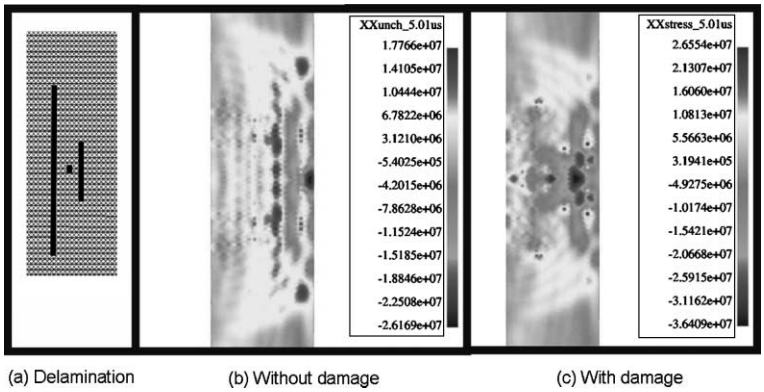

Fig. 14. Damage initiation and stress wave distribution at 5.01 μs after initial impact.

open, but may not be true for a closed delamination, where friction or contact may allow limited shear stress transfer across the surfaces. There is, of course, no guarantee that the delamination will remain open throughout the history of the impact event. On the other hand, there is no possibility in the element-failure method for interpenetration of delamination surfaces in the event of a closing delamination. This is a significant advantage over the modeling of delamination by the use of conventional finite element techniques because local interpenetration of delamination surfaces will cause non-physical solutions and much computational time must be spent on contact iterations (Shen et al., 2001). The element-failure code may be modified to allow for shear stress transfer whenever the delamination is closed, but this was not done in the present work.

Finally, Figs. 13 and 14 show the delamination profiles and stress wave distributions for 4.36 and 5.01 μs respectively after initial application of the impact pulse. In Fig. 13(a), the two largest delaminations have joined together to form a single large delamination, while other delaminations have also increased in size. The final damage pattern is shown in Fig. 14(a) for 5.01 μs after impact. Subsequent to this, there are no further propagation of the existing delaminations and no formation of new delaminations, although the simulation was carried out until 8.0 μs.

6. Conclusion

A novel finite element method for analyzing initiation and propagation of delaminations in low-velocity impact-damaged composite laminates is presented. The method employs an element-failure algorithm in which the delamination crack surfaces are not explicitly modeled, but are simulated by a series of partially failed elements. Naturally, the approximation to a true crack or delamination becomes better with increasing mesh density and decreasing element sizes. When applied to analysis of fracture, delamination and damage in composites, the method has a few advantages which have not yet been fully explored. Since damage in composites often involve a multiplicity of modes such as matrix cracking, delamination, fibre breakage and so forth, generally the conventional fracture mechanics approach of explicitly modeling multiple cracks is not feasible due to its overwhelming complexity. Furthermore, the presence of some damage does not necessarily cause the composite structure to completely lose its ability to sustain loads. The element-failure concept therefore seeks to model this partial ability to sustain loads by incorporating the effects of the damage through modifying the nodal forces of the finite element containing the damage. This effective nodal forces approach eliminates the need to reduce the values of the elastic properties of the material, a process that can cause computational problems. In this paper, the element-failure method is demonstrated by an example of delamination initiation and propagation in low-velocity impact of a composite laminate. The delaminations are modeled by a series of failed elements, which permit transmission of compressive but not tensile stress waves across the delaminated surfaces. The results show a considerable difference in the distributions of stress waves if delamination damage is modeled. The issue of possible interpenetration of delamination surfaces does not arise when the element-failure method is used in this case. This is because the failed elements are still able to resist compressive loads across the delamination surfaces at any moment in the loading history, ensuring no spurious solutions involving interpenetrating surfaces. This is another advantage over the conventional method of explicitly modeling the delaminated surfaces, where considerable computational time is generally required to check for interpenetration. If interpenetration has occurred, then contact iterations must be performed to obtain physically admissible solutions. The element-failure code in this work has been validated by comparing the computed results of the stress wave distributions for a laminate with no damage, with those obtained using the commercial finite element software ABAQUS. A further demonstration of the developed element-failure code is the simulation of crack propagation of pre-notched specimens of an isotropic material under initial conditions of mode II loading. The numerical results showed that the cracks propagated at an angle of about 70° with

respect to the notches, in agreement with the experimental results of Kalthoff, who performed actual tests under similar loading conditions. Of the two criteria used to guide crack propagation direction, the maximum hoop stress criterion gave a better prediction of the fracture trajectory than the maximum principal stress criterion. In both cases, the T^* energy integral was used to determine the crack tip velocity from experiment data on the correlation between crack tip velocity and stress intensity factor. Finally, it should be noted that the element-failure algorithm could be extended to the prediction of fracture propagation in three-dimensional problems, both in isotropic and anisotropic materials. A consistent methodology for this has not yet been developed, but it is interesting to note that in three-dimensions, it may be relatively easier to predict certain types of damage such as delamination in laminated composites than to predict the general development of crack planes in isotropic materials. This is because in the former, fibre reinforcements generally provide more constraints to crack path propagation.

References

Atluri, S.N., 1982. Path-independent integrals in finite elasticity and inelasticity, with body forces, inertia, and arbitrary crack-face conditions. Engineering Fracture Mechanics 16 (3), 341–364.

Atluri, S.N., Nishioka, T., Nakagaki, M., 1984. Incremental path-independent integrals in inelastic and dynamic fracture mechanics. Engineering Fracture Mechanics 20 (2), 209–244.

Bakuckas Jr., J.G., Lau, A.C.W., Tan, T.M., Awerbuch, J., 1995. Computational methodology to predict damage growth in unidirectional composites—I. Theoretical formulation and numerical implementation. Engineering Fracture Mechanics 52 (5), 937–951.

Beissel, S.R., Johnson, G.R., Popelar, C.H., 1998. An element-failure algorithm for dynamic crack propagation in general directions. Engineering Fracture Mechanics 61 (3–4), 407–425.

Choi, H.Y., Wu, H.-Y.T., Chang, F.-K., 1991. A new approach toward understanding damage mechanisms and mechanics of laminated composites due to low-velocity impact: Part II—Analysis. Journal of Composite Materials 25, 1012–1038.

Dally, J.W., Fourney, W.L., Irwin, G.R., 1985. On the uniqueness of the stress intensity factor-crack velocity relationship. International Journal of Fracture 27, 159–168.

Dexter, R.J., O'Donoghue, P.E., 1993. Computational procedures and energy integral for dynamic fracture in viscoplastic materials. Engineering Fracture Mechanics 44 (4), 591–607.

Erdogan, F., Sih, G.C., 1963. On the crack extension path in plates under plane loading and transverse shear. ASME J. Bas. Eng. 85, 519–523.

Freund, L.B., 1990. Dynamic Fracture Mechanics. Cambridge University Press, Cambridge, UK.

Gosse, J.H., 2002. An overview of the strain invariant failure theory (SIFT). In: Chang, F.-K. (Ed.), Proc. 10th US-Japan Conf. Composite Materials. DEStech Publications, Lancaster, PA, pp. 989–997.

Hussain, M.A., Pu, S.L., Underwood, J.H., 1974. Strain energy release rate for a crack under combined Model I and Mode II. In: Fracture Analysis, ASTM-STP 560. American Society for Testing and Materials, pp. 2–28.

Kalthoff, J.F., 1988. Shadow optical analysis of dynamic shear fracture. Optical Engineering 27 (10), 835–840.

Kalthoff, J.F., Winkler, S., 1988. Failure mode transition at high rates of shear loading. In: Chiem, C.Y., Kunze, A.D., Meyer, L.W. (Eds.), Proc. Int. Conf. Impact Loading and Dynamic Behaviour of Materials. Deutsche Gesellschaft Metallkunde, Oberursel FRG, pp. 185–196.

Kanninen, M.F., Poplar, C.H., 1985. Advanced Fracture Mechanics. Oxford University Press, New York, Oxford.

Lim, I.L., Johnston, I.W., Choi, S.K., 1996. A finite element code for fracture propagation analysis within elasto-plastic continuum. Engineering Fracture Mechanics 53 (2), 193–211.

Mahishi, J.M., Adams, D.F., 1982. Micromechanical predictions of crack initiation, propagation, and crack growth resistance in boron/aluminum composites. Journal of Composite Materials 16, 457–469.

Murti, V., 1986. Numerical fracture mechanics using finite element methods. Ph.D. dissertation, University of New South Wales.

Rosakis, A.J., Freund, L.B., 1982. Optical measurement of the plane strain concentration at a crack tip in a ductile steel plate. Journal of Engineering Materials Technology 104, 115–120.

Rose, L.R.F., 1976. Recent theoretical and experimental results on fast brittle fracture. International Journal of Fracture 12, 799–813.

Rousselier, D., 1979. Numerical treatment of crack growth problems. In: Larsson, L.H. (Ed.), Advances in Elasto-plastic Fracture Mechanics, pp. 165–189.

Samoa, V.E., 1981. Interactive finite element analysis of reinforced concrete: A fracture mechanics approach. Ph.D. dissertation, School of Civil and Environmental Engineering, Cornell University.

Shen, F., Lee, K.H., Tay, T.E., 2001. Modeling delamination growth in laminated composites. Composites Science and Technology 61, 1239–1251.

Sih, G.C., 1974. Strain energy density factor applied to mixed-mode crack problems. International Journal of Fracture 10, 305–321.

Taha, N.M., Swartz, S.E., 1989. Crack propagation models for mixed-mode loading. In: Shah, S.P., Swartz, S.E., Barr, B. (Eds.), Fracture of Concrete and Rocks: Recent Developments. Elsevier Science, pp. 5–17.

Tay, T.E., Lam, K.Y., Cen, Z., 1997. Analysis of composite structures with distributed and localized damage by the finite-element method. Composite Structures 37, 135–143.

Tsai, S.W., 1992. Theory of Composites Design. Think Composites, Dayton.